Journal of Electroceramics 3:3, 279–299, 1999

Thermodynamic Stability and Interfacial Impedance of Solid-Electrolyte Cells with Noble-Metal Electrodes

VICTOR STANCOVSKI
Independent Consultant, Pasadena, CA

SEETHARAMAN SRIDHAR
Department of Materials, Imperial College of Science, Technology and Medicine, London, UK

UDAY B. PAL
Department of Manufacturing Engineering, Boston University, MA

Submitted May 27, 1998; Revised July 2, 1998; Accepted July 24, 1998

Abstract. In solid-electrolyte cells, the electrode-electrolyte interfacial stability and impedance are found to be dependent on temperature, atmosphere, current density, microstructure and the process history of the cell. The modifications induced by temperature and oxygen pressure on the impedance spectra of Pt/Yttria-stabilized zirconia (YSZ) and Pd/YSZ interfaces have been studied. The interfacial impedance was controlled by adsorption/desorption of oxygen with a Langmuir-type dependency. When the surface coverage was small, the interfacial impedance decreased with increase in temperature and P_{O_2}. In certain temperature and P_{O_2} regimes and depending on the process history, the metal electrode formed stable oxygen-containing species. In this region, the interfacial impedance increased markedly and its P_{O_2} dependence also changed. Anodic and cathodic currents altered the local thermodynamic conditions at the charge-transfer sites and accordingly influenced the interfacial impedance. The concentration of oxygen-containing species and the interfacial microstructure are shown to influence the shape of the impedance response. Pt was found to form a neck at the YSZ electrolyte and Pd did not. The electrode polarization in the case of Pt/YSZ interface corresponded to one impedance-response arc signifying charge-transfer resistance at the three-phase boundary (TPB), gas/Pt/YSZ interface. For the Pd/YSZ interface, the electrode polarization corresponded to two impedance-response arcs at low P_{O_2}. The high-frequency response is related to charge transfer at the TPB and the low frequency to the gas-phase mass transfer.

Keywords:

Introduction

In stabilized-zirconia-based electrochemical devices, understanding the nature of the reactions that occur at the three-phase boundaries (TPB) gas/electrode/stabilized-zirconia electrolytes is very important for identifying effective ways for decreasing the polarization losses and optimizing the electrode processes. The elementary steps of the reaction mechanism are not yet fully understood. The exact roles of the different phases (ionic/electronic/mixed conductors and gas) are not clear either. The work done over the last few decades in this area was more recently examined critically by a number of authors (Wiemhofer, [1,2], Barbi [3], Siebert [4], Steele [5], Schwandt and Weppner [6]) who pointed out the remaining uncertainties in understanding the elementary steps of the reaction mechanism. Moreover, the information available on the reaction mechanisms at the gas/electrode/electrolyte interface while current is passing is relatively scarce.

The study of noble-metal electrodes is directly applicable to the design of sensors and oxygen pumps since these devices frequently use such electrodes.

State-of-the-art SOFC (solid-oxide fuel cells) use Ni/ZrO_2 cermet anodes. It is difficult to quantify and characterize the TPB in the cermet structure. Furthermore, this structure is stable only under reducing atmospheres. The use of noble-metal electrodes offers an easily controllable electrode morphology. They are relatively stable in reducing as well as oxidizing atmospheres. If a mechanistic theory can be established for oxygen and charge transfer between electronic and ionic conductors through a study of noble metal/stabilized-zirconia interfaces, tailoring and optimizing the cermet structures may be possible.

The electrode/electrolyte interfacial impedance is influenced by the temperature and gas atmosphere. The stabilities of the electrode and electrolyte are also influenced by these variables as well. If the electrode and the electrolyte materials chemically react with the gas atmosphere and form compounds or species, then these materials are truly not inert and the interfacial impedance can be expected to markedly change. When the solid-oxide electrochemical cell is operating under a given load, the local current densities near the TPB, which depend on the microstructure, can change the oxygen-chemical potential to a significantly different value as compared to that in the bulk of the porous electrode. As a result, the interfacial impedance of the cell may change with the load.

Our initial work with a laboratory-scale solid-oxide electrochemical cell, consisting of Pt cathode, yttria-stabilized-zirconia (YSZ) electrolyte and Ni-YSZ anode, showed that the measured cell impedance was substantially altered after operating the cell under a specific load [7]. The impedance change was partially irreversible. In this process no visible changes in the microstructure of the electrode were observed. This behavior meant that current passage leads to irreversible changes of one or more processes responsible for the cell impedance. The consequence is that the electrochemical overpotential measurements that determine the polarization characteristics at different currents are not easily interpreted. Thus, the source of the current-induced effect on the impedance needs to be identified by experimentally isolating the interfaces.

A cell was constructed for the purpose of studying the effect of current on the noble metal/YSZ interfacial impedance as a function of temperature and oxygen partial pressure in the gas phase. A time-domain impedance spectroscopy technique was used for the study of the interfaces after current interruption [7]. It was observed that the local current-induced change in oxygen-chemical potential altered the oxygen-exchange rate at the electrode-electrolyte interface. The electrode morphology did not change.

Pt is generally thought to be inert with respect to high-temperature oxidation. However, there is sufficient evidence in the literature to suggest that various oxygen compounds form on the Pt surface. Relevant available thermodynamic information on the Pt-O system is presented below.

Platinum-oxygen system. Pt is known for its resistance to oxidation. Figure 1(a) shows a plot of the standard Gibbs free energy of formation for a number of platinum oxides with various stoichiometries at 1 atm pressure as a function of temperature [8]. None of the oxides is thermodynamically stable above

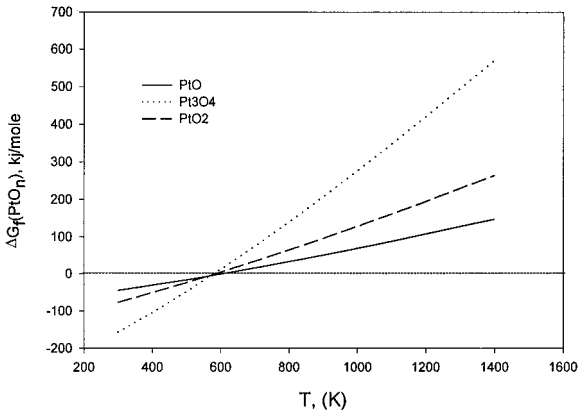

Fig. 1a. ΔG of formation of PtO_n in 1 atm O_2 vs. T.

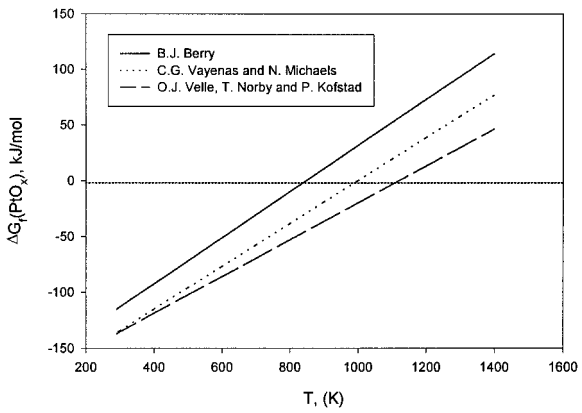

Fig. 1b. ΔG of formation of PtO_x in 1 atm O_2 vs. T.

300°C, and it is likely that their nucleation will be kinetically hindered below 300°C. These oxides can therefore be assumed to be non-existent in the temperature and pressure conditions at which YSZ-based devices operate.

Even though Pt is resistant towards bulk oxidation, there is in surface science and catalysis literature enough evidence to suggest that Pt is not entirely inert with respect to forming interfacial and surface bonds with oxygen.

Gland et al. [9,10] studied the interaction of Pt single crystals (Pt(111)) with oxygen over a wide temperature range (− 173 to 1127°C) by using *in situ* spectroscopic techniques (EELS, UPS, TDS, XPS and AES) and identified three states of oxygen on the Pt(111) surface. The first state is observed below − 100°C, where adsorbed molecular oxygen predominates with a desorption heat of 37 kJ/mole. The second state is between − 123 to 427°C, where adsorbed atomic oxygen predominates. The heat of adsorption varies with the coverage, i.e., at a coverage $\theta = 0.02$ the heat is around 500 kJ/mole, and it is 160 kJ/mole at $\theta = 0.8$. The third state is found at higher temperatures, between 527–827°C, where a *subsurface* oxygen is present. Its decomposition begins near 977°C and the process is limited by mass transfer. The authors were not able to obtain the decomposition heats.

Somorjai [11] reported that the thermal desorption of oxygen from a Pt-crystal surface (12,9,8) has two maxima, one at 700–800°C and the other at 950–1000°C. The heat of adsorption of the strongly-bound oxygen was estimated to be 270 kJ/mole. Kuzin and Komarov [12] studied the adsorption of oxygen on porous Pt electrodes between 552–758°C and found two states of oxygen, a weakly bound adsorbed state and a strongly bound one. Pt-O compounds that are stable at high temperatures have been found by several other investigators [13–15]. The stoichiometry for these oxides has not been established. The free energy diagrams for these oxides are shown in Fig. 1(b).

The effect of temperature, oxygen partial pressure, and current on the interfacial impedance was correlated to the stability of oxygen-containing species (OCS) on platinum. Based on these results, a hypothesis was formulated that the oxygen transfer process is slowed by the presence of the OCS at the oxygen-transfer sites. The hypothesis was then tested on the Pd/YSZ system by conducting a similar set of experiments. Available thermodynamic information on the Pd-O system is presented below.

Palladium-oxygen system. Pd differs from Pt in that a stable oxide (PdO) is present in a wide P_{O_2} and temperature range, as shown in Fig. 2. The kinetics of Pd oxidation has been reported by Duval [17]. In air, Pd oxidation starts above 364°C and decomposes over 830°C. Badwal et al. [18] investigated the electrode kinetics at the Pd/YSZ interface in the temperature range 600–1000°C. They observed steep changes in electrode resistance upon thermal cycling around the decomposition temperature of PdO. The reaction model proposed to explain these observations assumes that the oxygen charge transfer reaction takes place at the PdO/YSZ interface; PdO is an intrinsic semiconductor above 250°C and may act as an electron source/sink. The low-frequency-impedance spectra indicate the presence of a sequence of processes with partially overlapping time constants. Such processes can be related to a multistep redox reaction in which the intermediate products are relatively stable. The authors suggest that, beyond its role as electron sink/source, the noble metal participates in its own redox processes.

In the present paper the oxygen compounds of Pd are referred to as oxygen-containing species of Pd.

Role of oxygen-containing species at the metal/YSZ interface. As discussed earlier, it is possible that oxygen may react with Pd or Pt at the surface to form oxygen-containing species of varying stability. For Pd

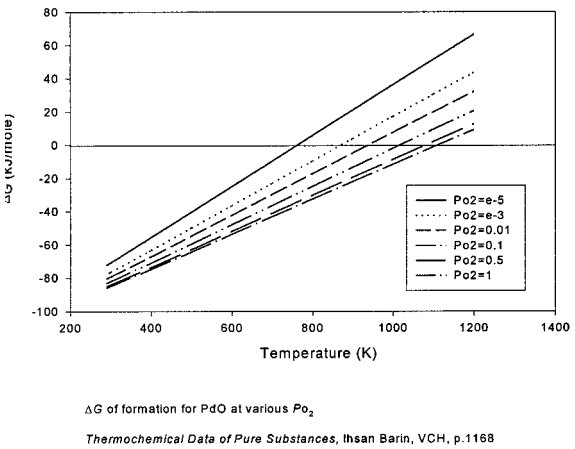

Fig. 2. ΔG of formation of PdO vs. temperature of various P_{O_2} (calculated with data from [16]).

there exists a definite oxide, whereas, for Pt, there exists a range of adsorbed oxygen species including subsurface oxygen. Any type of oxygen bonded to the metal will henceforth be denoted, *oxygen-containing species* or OCS.

The OCS may form from oxygen supplied from the atmosphere or from an anodic current. As shown in Fig. 3, the oxygen-transfer reaction takes place at or near the triple-phase boundary (TPB). The presence of OCS at the TPB may block the reaction if it is insulating. On the other hand, if the OCS is susceptible to dissociation, it may only be partially blocking. The OCS may then act as an intermediate step in the charge-transfer process. Therefore, the interfacial process involving the OCS can be electrically associated with an impedance Z_{OCS}. The magnitude of Z_{OCS} depends on the strength of the O bonds that need to be broken or established in the oxygen-transfer process. TPB sites covered with OCS may coexist with clean TPB sites. Under such circumstances two paths may exist for oxygen transfer: one through the OCS and another at the OCS-free TPB sites.

Experimental

A three-electrode system, with counter, working, and reference electrodes were used in order to isolate the impedance response of a single electrode/electrolyte interface. The experimental setup is shown in Fig. 4. The EIS study was carried out with a Solartron 1260 Impedance Analyzer controlled by the Z60 software written by Scribner Associates. The spectra were taken over the frequency range 80,000 Hz–1 Hz and had a total integration time of 1 min. The impedance analyzer was operated in voltage-control mode; the ac amplitude used (30 mV), was validated by linearity checks.

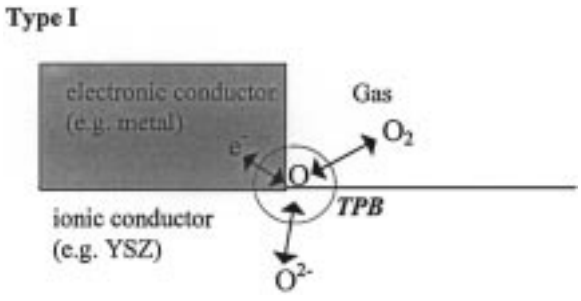

Fig. 3. The triple phase boundary (TPB).

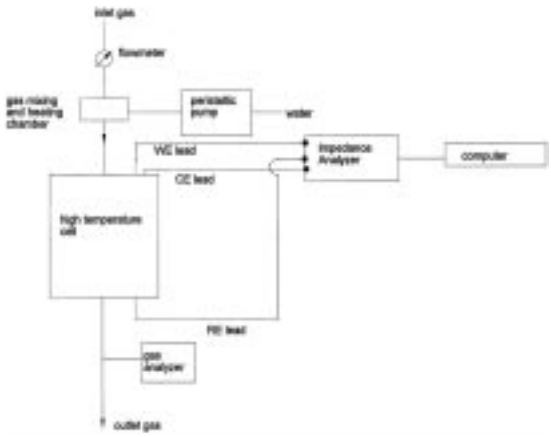

Fig. 4. The experimental setup for 3-electrode impedance measurement of a YSZ/electrode interface.

The YSZ (8 mole % yttria-stabilized zirconia) electrolyte disks, 1.25 cm in diameter and 0.17 cm thickness, were supplied by Siemens AG (Germany). The working (WE) and counter (CE) electrodes were stenciled on opposite sides of the solid electrolyte (YSZ) disc with either platinum or palladium inks. The reference electrode was coated with the same material on the edge of the YSZ disc. The thickness of the electrodes were 1–15 microns. Before applying the Pt or the Pd ink, the electrolyte surfaces were polished and washed in an ultrasonic bath, first with acetone then with de-ionized water. The Pt ink was supplied by Engelhard Company (Pt-ink 6926). After applying the Pt ink, the samples were air-dried for 24 h and then fired in air at 900°C for 1.5 h. This material does not contain inorganic additives that might result in oxide phases at the interfaces in the system. The Pd inks, supplied by Engelhard Company, were heated in air to above 600°C for 1.5 h in order for the binder material to burn off completely. This process was found to generate PdO. Therefore, in order to decompose the oxides of Pd following the binder burn-off, the material was heated in Ar to 900°C for 24 h. Thermogravimetric experiments were performed to confirm the formation and decomposition of the PdO. The minimum distance between the RE-WE and RE-CE, respectively, was 2 mm. The contacts between the electrodes and lead wires were achieved by platinum mesh (with approximately 1 mm size square openings) pressed on to the

electrodes by alumina wedges. This configuration maintained a good electrical contact and permitted free access of the gas phase to the electrodes while allowing for thermal expansion. The cross section of the cell is shown in Fig. 5.

The high-temperature cell was placed inside an alumina tube sealed with steel-end caps having openings for gases, thermocouples and electrical leads. This entire assembly was placed inside a resistance-heated Lindbergh furnace with a 12 inch hot zone. Care was taken so that the cell was placed in the middle of the hot zone of the furnace. Gas flow rates were selected such that the gases would reach the furnace temperature at the beginning of the hot zone and would not alter the temperature of the cell. The inlet gases were set by calibrated flowmeters supplied by Alborg and Matheson. The P_{O_2} was established by using pure Ar (grade 5) or Ar-air mixtures. The oxygen partial pressure of the Ar in the gas cylinder was checked in our laboratory with an oxygen sensor and was found to be on the order of 10^{-6} atm. The partial pressure of the exit Ar from our system was measured with a mass spectrometer and found to be 10^{-5} atm.

The interfaces under study were placed in gas mixtures of known P_{O_2} and were monitored until a steady state, as seen by EIS, was reached. After observing a stable spectrum for a given P_{O_2}, small currents ($< 10\,\text{mA/cm}^2$) were passed. While the current passes, the WE functions as a cathode or an anode, depending on the direction of the current. Impedance spectra were taken at short intervals after current interruption. The frequency response of the interface was thus monitored in the time domain. The effect of long exposure (24 h and more) of Pt electrodes to larger anodic currents has been studied by Van Herle et al. [19] and was shown to lead to the doubling of the polarization resistance (R_p). This effect was attributed to the sintering of the porous

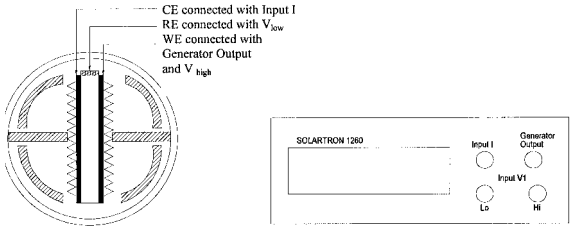

Fig. 5. The high-temperature cell and the connections of the electrodes to the terminals of the Solartron 1260.

platinum. The situation analyzed in this work is different. In order to avoid the sintering of the electrode, much lower current densities and significantly shorter exposure times were used in our work. The microstructure of the Pt electrode after the experiment was found to be the same as compared to the one observed before [20].

Theory

The Complexity of the Oxygen-Transfer Reaction

The oxygen-exchange reaction at the metal electrode/YSZ electrolyte interface can be represented as follows:

$$O^{2-} + V_{ads} \Leftrightarrow 2e^- + O_{ads} \tag{1}$$

The above reaction involves the participation of ionic oxygen, atomic oxygen, vacant adsorption sites, and electrons. The idle rate of this reaction can be represented by the exchange current.

$$I_0 = f(n, A, T, [V_{ads}], [O_{ads}]) \tag{2}$$

Mechanistically this is a complex problem to analyze, particularly because the reaction sites are not of a simple nature and they are hard to identify. Even more difficult is quantifying the effective reaction area, A. The existing models are based on measurements under static conditions, i.e., zero-current flow. As mentioned earlier, it is likely that the electrodes are affected by changes in the local oxygen-chemical potentials induced by the passage of a current.

The solubility of oxygen is generally low in noble-metal-electrode phase, and thus, the exchange reaction occurs mainly at the surface in a sorption layer. There are many proposed models, but it is generally agreed that the actual charge transfer occurs at or near the triple-phase boundaries (electronic conductor/ionic conductor/gas).

With respect to Eq. (1), the schematic in Fig. 6 represents the cathodic-charge-transfer reaction. The rate-limiting step for the oxygen transfer may be one or more of the steps shown in Fig. 6 (Etsell and Flengas [21], Gur et al. [22], Braunshtein et al. [23], Anderson [24], Bauerle [25], Moghadam et al. [26], Pizzini [27], Mizusaki et al. [28], Wang and Nowick [29]). The objective of this work is to connect the interfacial impedance response to the various kinetic processes presented in Fig. 6 and elucidate the role of

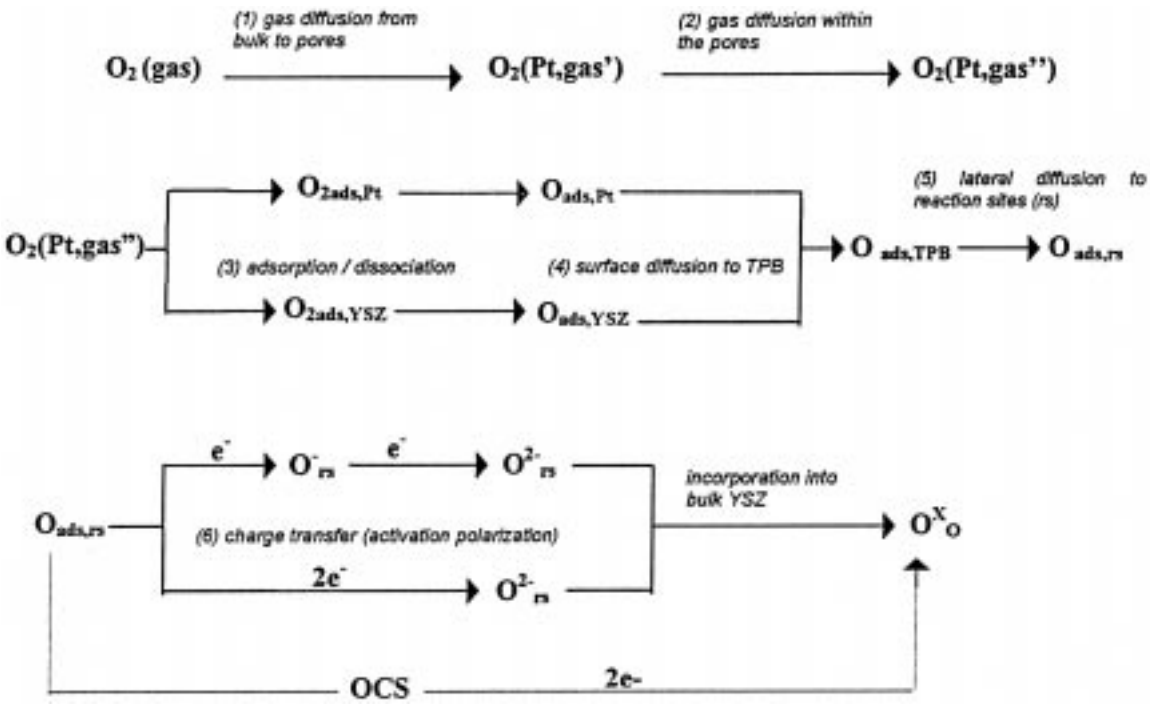

Fig. 6. Schematic of the pathways of oxygen and charge transfer at the Pt/YSZ interfaces.

the OCS in the charge-transfer process. The reaction scheme presented in Fig. 6 has platinum as a metal electrode, but the scheme can be viewed as more general and hence applicable to any metal (including Pd) that does not dissolve oxygen appreciably.

Electrical Analogs of Physicochemical Processes at YSZ/Metal Interfaces

The YSZ/metal interface can be characterized as an electrical circuit consisting of a double layer capacitance in parallel with a faradaic impedance, as shown in Fig. 7 [30,31]. The double layer capacitance, C_{dl}, for the YSZ/Pt interface has been reported by many investigators (Winnubst et al. [32], Bauerle [25], Ververk and Burggraaf [33], Velle et al. [15]), and the values lie between 60–350 μF/cm^2. No P_{O_2}

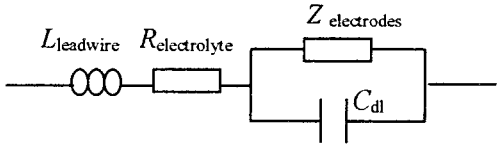

Fig. 7. Electrical circuit for the impedance of the overall cell and leads.

dependence has been observed. The faradaic impedance, Z_f, can be separated into two parts, charge transfer (R_{ct}) and mass transfer (Z_{mt}); $Z_f = R_{ct} + Z_{mt}$.

Charge-transfer resistance (R_{ct}). R_{ct} is related to step 6 in Fig. 6, and is given by:

$$R_{ct} = \frac{1}{\left(\frac{\partial i_f}{\partial V}\right)_\theta} \tag{3}$$

where θ corresponds to the surface coverage. If the relaxation frequency is high, the charge-transfer resistance can be isolated in the impedance spectra. Pure charge transfer is only encountered if the ac frequency is sufficiently high so that $\theta = \theta_{eq}$. θ_{eq} is the fraction of surface sites that are covered with adsorbed oxygen at near-equilibrium conditions.

The Butler-Volmer form for Eq. (1) is:

$$i_f = i_0 \left\{ \frac{1-\theta}{1-\theta_{eq}} \exp\left(\frac{\alpha_a n F \eta}{RT}\right) - \frac{\theta}{\theta_{eq}} \exp\left(\frac{-\alpha_c n F \eta}{RT}\right) \right\} \tag{4}$$

Here, α_a and α_c are the anodic and cathodic transference coefficients, respectively. η is the over-

potential. i_0 is the exchange current which can be shown to be [34]:

$$i_0 = nFAk_r(1-\theta_{eq})^{\alpha_c/\alpha_a+\alpha_c}(\theta_{eq})^{\alpha_a/\alpha_a+\alpha_c} \tag{5}$$

Here n is the number of electrons transferred and k_r is the rate constant for the idle reaction. $k_r = k_r^0 \exp(-E_r/RT)$, where k_r^0 is a constant and E_r is the activation energy of the idle reaction. Near equilibrium, when $\Delta\theta$ is small, Eq. (4) can be written as:

$$i_f = i_0\left\{\exp\left(\frac{\alpha_a nF\eta}{RT}\right) - \exp\left(\frac{-\alpha_c nF\eta}{RT}\right)\right\} \tag{6}$$

From Eq. (3) and Eq. (6) and assuming that the overpotential η is small, R_{ct} is readily evaluated:

$$R_{ct} = \frac{RT}{nFi_0(\alpha_a+\alpha_c)} \tag{7}$$

Note that Eq. (7) includes the exchange current given by Eq. (5). Since θ_{eq} represents the equilibrium coverage, it is set by the oxygen-chemical potential in the gas phase through an adsorption isotherm. Assuming a Langmuir-dissociative-adsorption isotherm for oxygen adsorption on metals, the equilibrium can be written as:

$$\frac{\theta_{eq}}{1-\theta_{eq}} = K_{diss}(P_{O_2})^{1/2} \quad \text{[dissociative]} \tag{8}$$

After inserting Eq. (8) in the expression for the exchange current in Eq. (5), two different forms of Eq. (7) can be written.

The form under high coverage ($\theta_{eq} \approx 1$) is:

$$R_{ct} = \frac{RT}{(\alpha_a+\alpha_c)n^2F^2\,Ak_r(K_{diss}P_{O_2})^{-\alpha_c/2(\alpha_c+\alpha_a)}} \tag{9}$$

and, under low coverage ($1-\theta_{eq} \approx 1$) is:

$$R_{ct} = \frac{RT}{(\alpha_a+\alpha_c)n^2F^2\,Ak_r(K_{diss}P_{O_2})^{\alpha_c/2(\alpha_c+\alpha_a)}} \tag{10}$$

The dependence of $\ln(R_{ct})$ on $1/T$ would reveal an apparent activation energy Q, which is a sum of the activation energy of the exchange current E_r and a contribution from the heat of adsorption ($K_{ads} = K_0 \exp(\Delta H_{ads}/(RT))$. The heat of adsorption is the negative of the free enthalpy change for equilibrium ($\Delta H_{ads} = -\Delta H$).

$$Q = \left(\frac{\partial \ln(R_{ct})}{\partial 1/T}\right) = E_r \pm \left(\frac{\alpha_c}{\alpha_c+\alpha_a}\right)\frac{\Delta H_{ads}}{2} \tag{11}$$

The sign in front of the second term is positive in the case of a high surface coverage ($\theta_{eq} = 1$) and negative for a low surface coverage ($1-\theta_{eq} = 1$).

According to this model, a plot of $\ln(R_{ct})$ versus P_{O_2} would have a negative slope at low coverage (low P_{O_2}'s) and a positive slope at high coverage (high P_{O_2}'s). The slope is defined by α_a and α_c, which depend on the slowest step of a multistep-charge-transfer process.

Mass-transport impedance Z_{mt}. The mass-transport impedance, Z_{mt}, is given by:

$$Z_{mt} = -\frac{\left(\frac{\partial i_f}{\partial \theta}\right)_V \frac{\Delta\theta}{\Delta i_f}}{\left(\frac{\partial i_f}{\partial V}\right)_\theta} \tag{12}$$

The denominator is evaluated from Eq. (6) and the first term in the numerator from Eq. (4). The second term, $\Delta\theta/\Delta i_f$, is obtained by solving an equation for the mass transport step (shown in Fig. 6) with appropriate boundary conditions [20].

Gas-phase diffusion (steps 1 and 2 in Fig. 6). Step 2 is usually slower compared to step 1. If the electrode is sufficiently porous and the thickness is very small, steps 1 and 2 are not expected to be rate controlling [28] at high P_{O_2}'s in near-equilibrium conditions. However, step 2 may explain the mass transfer-limited response of our impedance spectra when Pd is used as an electrode. This possibility is discussed in detail later in the paper.

Dissociative adsorption of atomic oxygen (step 3 in Fig. 6). If the adsorption/desorption step is not fast compared to the diffusion and charge transfer, Z_{mt} will depend on the kinetics of equilibration between oxygen in the gas phase and the adsorbed state. Franceschetti [35] developed a model consisting of an RC parallel circuit. R was inversely proportional to the kinetic rate constant for equilibration with the gas phase ($k_{eff} = |k_{adsorb} - k_{desorb}|$). The origin of C is unclear although it may be related to the fact that dissociated oxygen atoms tend to be negatively charged.

$$Z_{mt} \propto \frac{1}{k_{eff}} \tag{13}$$

Surface diffusion towards triple-phase boundary (step 4 in Fig. 6). The situation is illustrated in Fig. 8. The assumption is that adsorbed oxygen atoms have to diffuse a distance δ to the triple phase boundary on the surface of the electrode. Physically, the metal grain may have a very low contact angle with the electrolyte such that gas access to the TPB is prohibited in this region. At any distance from the triple-phase boundary beyond δ, the adsorption equilibrium holds, and therefore the surface coverage of oxygen atoms is in equilibrium with the gas phase, $\theta - \theta_{eq} = \Delta\theta = 0$. Hence, the first boundary condition becomes: $\Delta\theta_{(x=\delta)} = 0$. The current at the triple-phase boundary gives rise to a constant-flux boundary condition: $i_f = -2FD\Gamma\left(\frac{d\Delta\theta}{dx}\right)_{x=0}$. Γ is the oxygen activity when the fraction of surface coverage equals 1. D is the diffusion constant for oxygen. With these boundary conditions, Z_{mt} is obtained from Eq. (12).

$$Z_{mt} = \frac{RT}{4F^2 D\Gamma\theta_{eq}(1-\theta_{eq})}\frac{\tanh\left(\delta\sqrt{\frac{j\omega}{D}}\right)}{\sqrt{\frac{j\omega}{D}}} \tag{14}$$

Interfacial diffusion in the metal/YSZ -2 phase region (step 5 in Fig. 6). In the preceding two cases (steps 3 and 4) the charge-transfer kinetics is much faster than the mass-transport step. For a cathodic current, this would mean that any oxygen arriving at the triple-phase boundary is consumed immediately. There is no lack of reaction sites, and most of the charge-transfer reaction is located near the triple-phase-boundary region. If the charge transfer were not infinitely fast compared to steps 3 and 4, there would be a pile-up of oxygen near the three-phase interface (Fig. 9(a)). Wang and Nowick proposed that in the case of comparable charge-transfer and mass-transport rates, oxygen atoms would diffuse through the 2-phase region of the YSZ/metal interface, and thereby extend the reaction zone as shown in Fig. 9(b) [36].

An expression for the impedance, based on the competitive interfacial diffusion/charge transfer process, is shown in Eq. (15) [35]. The derivation was made with the assumption that the contacts between YSZ and metal grains are rectangular strips with widths of 2L (Fig. 10). k is a kinetic rate constant and D is the diffusion constant for oxygen in the 2-phase region.

$$Z_f = \frac{R_{ct}\left(1+\frac{j\omega}{k}\right)}{\left(\frac{j\omega}{k} + \left(\sqrt{\frac{kL^2}{D}\left(1+\frac{j\omega}{k}\right)}\coth\left(\sqrt{\frac{kL^2}{D}\left(1+\frac{j\omega}{k}\right)}\right)\right)^{-1}\right)} \tag{15}$$

Equation (15) includes the combined contribution of the mass transport and charge transfer. The complex

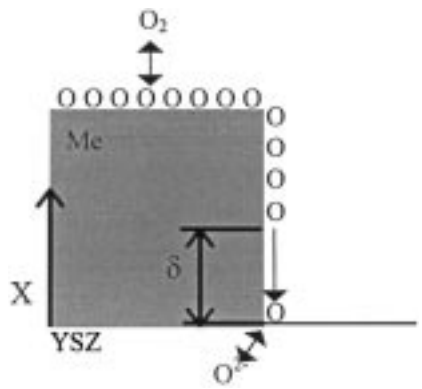

Fig. 8. Surface diffusion of atomic oxygen adsorbed on metal particle.

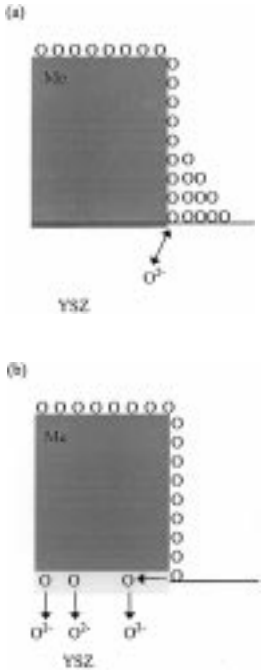

Fig. 9. Mass-transport rate is comparable to charge transfer rate. (a) Pile-up at the interface, (b) Interfacial diffusion model of Wang and Nowick [36] (dotted region represents the YSZ/metal interface).

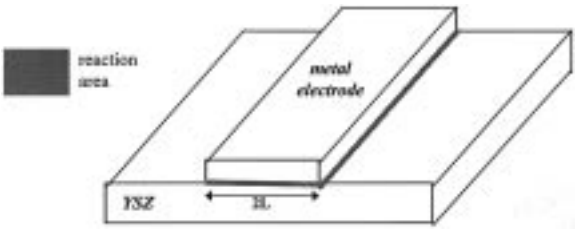

Fig. 10. The two-phase reaction zone.

nature of the impedance makes it hard to break down the expression into discrete components. At high frequencies however, Z_f will approach R_{ct}. Also, when the ratio L^2/D gets smaller, the diffusion will be faster, and Z_f will approach R_{ct}. Thus, when the metal particle size is small enough, the contribution of lateral diffusion will be negligible.

Results and Discussion

Platinum-YSZ Interface

Microstructure. The microstructure of the electrode is shown in Fig. 11. The cross-section of a fractured portion of the Pt/YSZ interface shows many contact points between Pt and YSZ (Fig. 11(b)). Necks seem to form at the contact points between Pt and YSZ. As seen from Fig. 11(b), the neck regions are directly accessible by gas (due to the open porosity). Therefore, the TPB where the oxygen transfer occurs must be located at these neck regions.

Effect of P_{O_2} and temperature. The interfacial impedance near equilibrium conditions was measured in the temperature range, 650 to 900°C, and P_{O_2} range, 0.01 to 1 atm. A single depressed arc was observed in the frequency region assigned to the interfacial-oxygen-charge-transfer reaction. R_p (the difference in the real axis intercepts of the arc) is plotted as a function of P_{O_2} on a natural-log scale in Fig. 12. The results of the relationship between R_p and P_{O_2} are summarized in Table 1; $R_p = (P_{O_2})^m$. m is negative, which means that R_p decreases with increasing P_{O_2}. The results agree with the Langmuir dissociative adsorption model with low surface coverage as given in Eq. (10). At 900°C, m is about half of what is observed at lower temperatures. The heat of dissociative adsorption for oxygen on platinum is 294 kJ/mole [24]. The activation energy calculated with Eq. (11) then becomes 208 ± 5 kJ/mole.

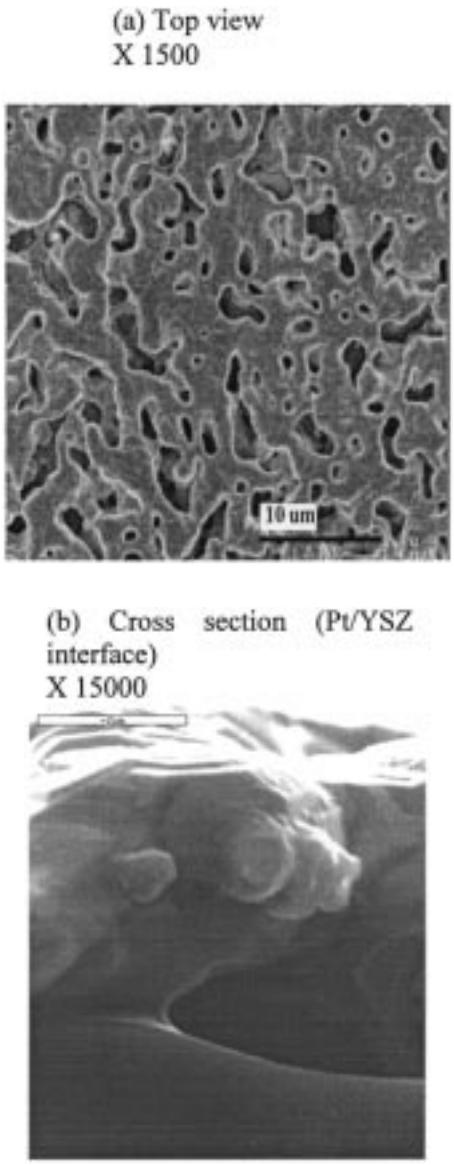

Fig. 11. The Pt electrode and the Pt/YSZ interface.

Table 1. Summary of near-equilibrium-impedance measurements of the Pt/YSZ interface

Element	Q (kJ / mole)	m, $[R_p = (P_{E_2})^m]$
R_p	90 ± 5	−0.18 ± (0.01) ($T = 900$ °C) −0.41 ± 0.01 (T < 900°C)

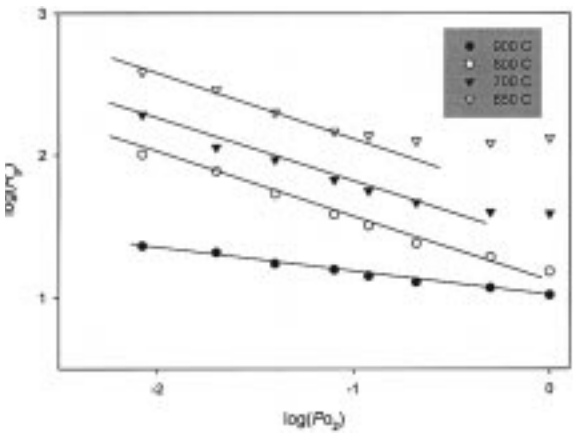

Fig. 12. $\log R_p$ vs. $\log(P_{O_2})$.

Effect of direct current. The changes in the electrode/electrolyte interfacial impedance with respect to the initial steady state were recorded after a small current $(5–10\,mA/cm^2)$ was applied. The applied currents were kept small so that the electrode microstructure does not change. After going through a transient period, the impedance spectrum evolved towards a new steady state. The new steady state was not identical to the initial one before the current was passed. The nature and magnitude of both the time-dependent and time-independent changes were found to be influenced by the oxygen partial pressure, direction of the current, temperature, current density, and the total charge passed.

Figure 13(a) shows the substantial change in the impedance spectra after the interruption of an anodic current of 10 mA passed for 10 min at 900°C and $P_{O_2} = 0.6$ atm. The change in the impedance spectrum is characterized by significantly larger values of the polarization resistance, R_p, and maximum absolute value of the imaginary component, Z''_{max}. Next, starting from this new steady state, a cathodic current of 10 mA is passed for 10 min (Fig. 13(b)). The new equilibrium spectrum measured after current interruption is ''shrunk.'' The new steady state is different from both the earlier measured steady states. Since the cathodic current does not totally restore the interface to the initial state, but leaves a hysteresis, it can be argued that the effect is not fully reversible. Immediately after interruption of cathodic or anodic currents there was a distinct time dependence of the spectra until the new equilibrium state was reached. Similar patterns of time evolution and the hysteresis

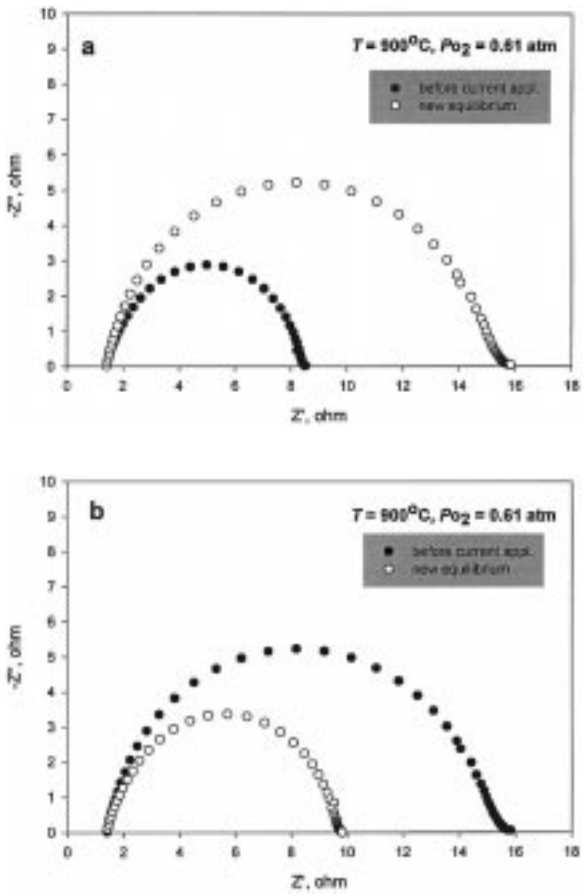

Fig. 13. Effect of: (a) an anodic current (10 mA) passed for 10 min; (b) a cathodic current (10 mA) passed for 10 min.

of the frequency response of the Pt/YSZ interfaces were also found to hold in other oxygen-rich atmospheres, such as $P_{O_2} = 0.08$ atm and 0.21 atm.

A different pattern of behavior was found in an oxygen-poor atmosphere (pure argon), as shown in Fig. 14(a) and 14(b). The equilibrium spectrum after the interruption of an anodic current does not differ much from the initial spectrum. After a cathodic current, the spectrum is ''shrunk'' (Fig. 14(b)). A significant difference is also found in the time scales required for reaching a steady state: 15–20 min in an oxygen-rich atmosphere and more than 100 min in an oxygen-poor atmosphere.

Effect of process-temperature history. During heating the system from room temperature to 1050°C in air and its subsequent cooling to room

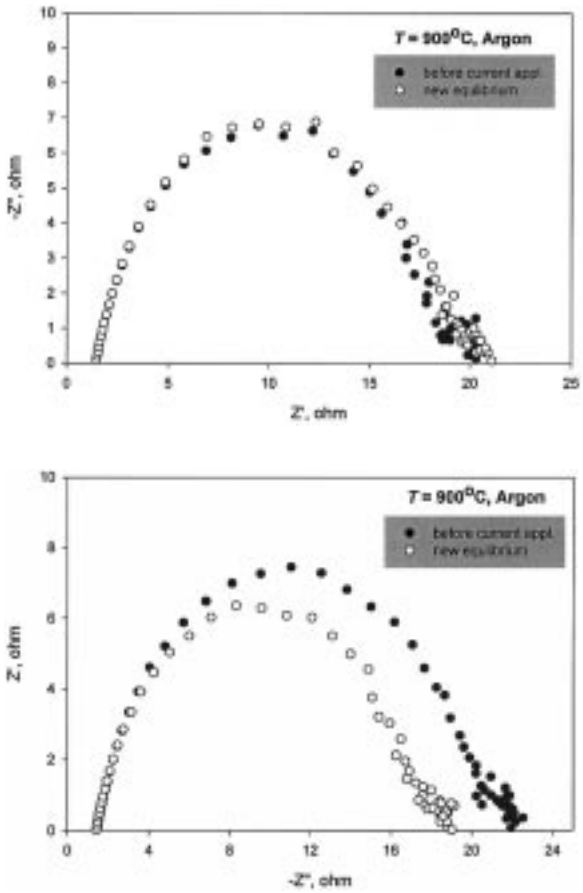

Fig. 14. Effect of: (a) an anodic current (10 mA) passed for 10 min; (b) a cathodic current (10 mA) passed for 10 min.

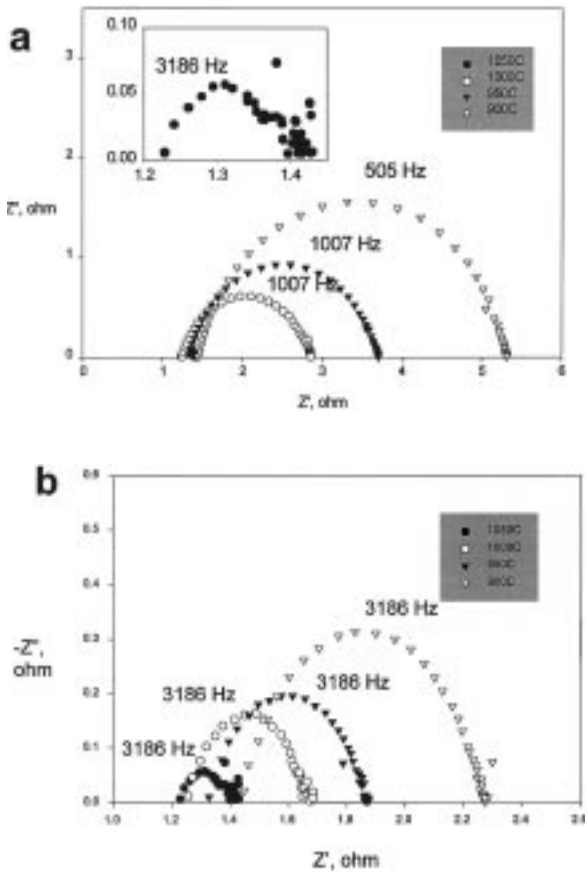

Fig. 15. Steady-state spectra between 1050°C and 900°C: (a) heating from room temperature; (b) cooling from 1050°C.

temperature, distinctly different behaviors in the frequency response of the Pt/YSZ interface were encountered between 850°C–1000°C.

Figure 15(a) shows the interfacial impedance spectra in air for the temperature range $1050°C \geq T \geq 900°C$ upon heating from room temperature. Figure 15(b) shows the corresponding spectra after the cell has been heat-treated at 1050°C and then cooled to the same temperature interval. As seen in Fig. 15, the 1050°C treatment resulted in decreasing the interfacial impedances observed during cooling. Although, the frequency of the maximum of the imaginary part of the impedance, $f_{Z''_{\max}}$, remained the same. This meant that the dominant reaction mechanism remains the same throughout the cooling process. On the contrary, Fig. 15(a) shows that $f_{Z''_{\max}}$ during heating from room temperature has a temperature dependence and a smaller value compared to Fig. 15(b). This suggests that the oxygen-charge-transfer reaction mechanism in Fig. 15(a) changes with temperature and is slower compared to that shown in Fig. 15(b). This is further supported by the fact that the spectra in Fig. 15(b) took about 10–30 min to attain steady state after reaching the desired temperature, whereas when heating from room temperature (Fig. 15(a)), it took considerably longer for the spectra to attain a steady state (5–20 h).

The direct current-induced change in the impedance spectra that was discussed earlier was also studied as a function of process-temperature history. This effect was not observed in the temperature range $1050°C > T > 850°C$ after the 1050°C treatment. Below 850°C, however, the direct current-induced modification of the impedance spectra was observable. The influence of the thermal-history conditions on the current-induced modification of the impedance spectra is summarized in Fig. 16.

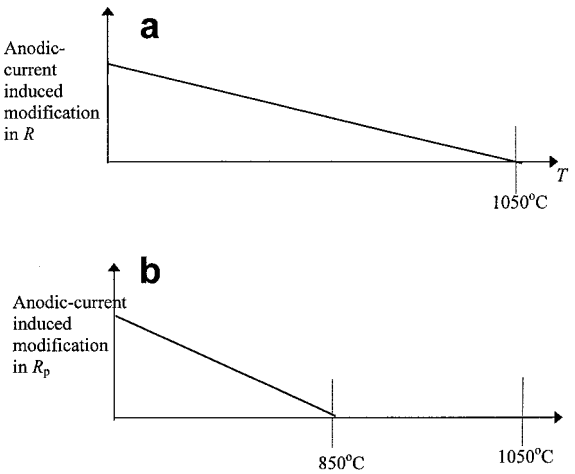

Fig. 16. Thermal conditions for current-induced effect: (a) heating from room temperature; (b) cooling from 1050°C.

Physico-chemical model. In oxygen-containing atmospheres under open-circuit conditions at a given temperature, the oxygen in the gas phase and the adsorbed oxygen atoms on the electrode surface will try to equilibrate according to:

$$O_{2,gas} \leftrightarrow 2\,O_{ads} \tag{16}$$

As suggested in the section on ''Pt-O System'' the O_{ads} species can also be loosely and reversibly bound at certain sites, including the three phase boundaries (TPB):

$$O_{ads} + (Pt)_n \leftrightarrow (Pt)_n \cdots O \tag{17}$$

The transformation of these reversible sites into more stable, partially-oxidized species is possible as well:

$$(Pt)_n \cdots O \leftrightarrow (Pt)_n O \tag{18}$$

OCS includes all types of oxygen species present at the electrode from weakly adsorbed oxygen atoms to stable oxides. When OCS are present at the TPB, they will decrease the number of clean-effective-charge-transfer sites, and thereby increase the interfacial impedance and vice-versa. The equilibration processes for reactions 16–18 is expected to be time-dependent and a function of temperature, process history and P_{O_2}. As a result, the equilibration of the interfacial impedance is also found to be time-dependent and is similarly influenced by the same set of variables.

Current passage changes the local oxygen concentration at the TPB, which may also change the concentrations of the $(Pt)_n^{\bullet\bullet} O$ and $(Pt)_n O$ species, according to the following reactions:

$$(Pt)_n \cdots O + 2e^- \leftrightarrow (Pt)_n + O_{TPB}^{2-} \tag{19}$$

$$(Pt)_n O + 2e^- \leftrightarrow (Pt)_n + O_{TPB}^{2-} \tag{20}$$

From Eqs. (19) and (20), it can be seen that an anodic current (oxygen is supplied to the TPB from the direction of the YSZ electrolyte) will lead to the formation of OCS and a decrease in the number of clean-charge-transfer sites, thereby inhibiting the oxygen-transfer reaction. A cathodic current (oxygen is extracted from the TPB and incorporated into the YSZ electrolyte) will decompose the OCS, increase the concentration of clean-charge-transfer sites, and lead to more effective electrocatalysis. The proposed model is described in Fig. 17 and agrees with the observed impedance spectra in oxygen-rich atmospheres. The current-induced modification has a time-dependent recovery of the impedance that takes place after current interruption. During the time-dependent recovery of the impedance, the OCS concentration tries to re-equilibrate with the gas phase.

In pure argon ($P_{O_2} = 10^{-5}$ atm), the current-induced modification of the impedance spectra is not very prominent (see Fig. 14). The reason is that in oxygen-poor atmospheres, the steady-state concentrations of the $(Pt)_n^{\bullet\bullet} O$ and $(Pt)_n O$ species are already

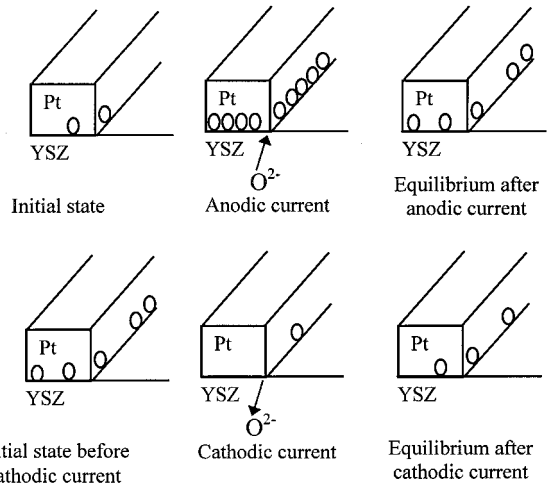

Fig. 17. Current-induced oxygen supply/depletion at the TPB.

very low and the steady-state polarization resistance is fairly large due to the low P_{O_2}.

The heat treatment at 1050°C results in a gradual decrease in R_p as shown in Fig. 18. Keeping the interface at 1050°C for a sufficiently long interval of time ($\cong$1000 min) ultimately results in stripping most of the OCS via its decomposition. Somorjai [11] and Gland et al. [9,10] have reported that subsurface oxides in Pt decompose at around 980°C. By heating to 1050°C we may be providing the necessary activation energy for the complete decomposition of the OCS. As mentioned earlier, the current-induced modification of the impedance is not observed upon cooling from 1050°C to 800°C (Fig. 16). It is conceivable that once all the OCS have decomposed at 1050°C, the OCS surface coverage becomes very low. Then, during cooling to 800°C, sufficient OCS do not nucleate to substantially change the surface coverage even when small anodic currents are passed. As a result, no visible current-induced modification of the interfacial impedance is observed during this cooling process. However, when the temperature is below 800°C, it is possible that sufficient OCS are formed and that the oxygen-exchange reaction is primarily controlled by the smaller fraction of the clean sites. In this regime, when some more OCS are generated by small anodic currents, this further decreases the fraction of clean sites and thus influences the interfacial impedance. Therefore, when heating from lower temperatures (below 800°C), where sufficient OCS are formed and are thermodynamically stable up to 1050°C, current-induced modification of the impedance spectra is present all the way up to 1050°C.

The activation energy for the overall polarization R_p in the temperature range 800°C $< T <$ 1050°C is approximately 80 kJ greater when heating from room temperature (Fig. 15(a)) compared to when cooling from 1050°C (Fig. 15(b)). This is of the same order of magnitude as the enthalpy of formation for PtO (71.18 kJ/mole) [8].

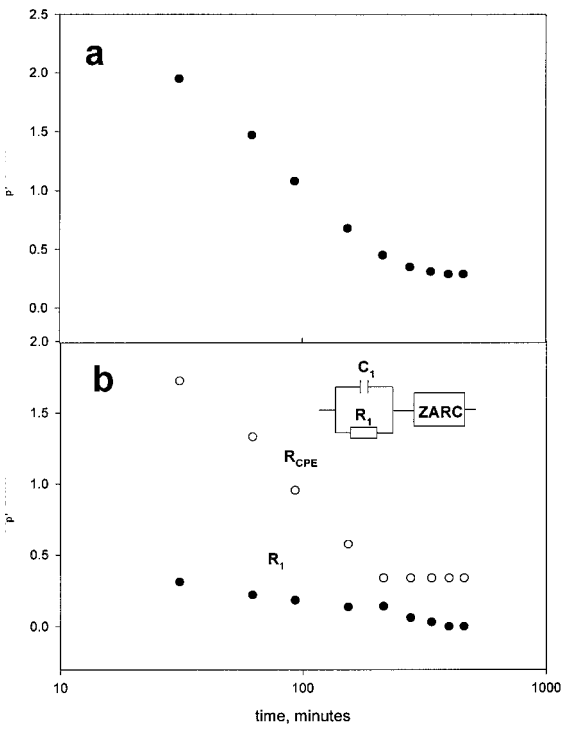

Fig. 18. Evolution of the impedance spectra of the Pt/YSZ interface during heat treatment at 1050°C: (a) total R_p; (b) the R values from a R-C element and from a distributed element. The last spectra are best fitted with a ZARC only; the R-C element tends to become insignificant.

Palladium-YSZ Interface

In the case of Pt, a strong connection was made between the impedance of the Pt/YSZ interface and OCS. In this section, it will be shown that the oxygen-containing species, which in the case of Pd are its well defined oxides, cause similar effects and trends to be observed while measuring the interfacial impedance as a function of temperature, P_{O_2} and current.

Microstructure. Figure 19 shows the microstructure of the surface of the Pd coating and Fig. 20 shows fractured cross sections of the Pd/YSZ interface. The material is representative of the electrodes used in all the electrochemical measurements of the unoxidized Pd electrode. As seen from Fig. 19, the grains formed a continuous network on the electrolyte surface. In contrast to the Pt/YSZ interface, portion of the Pd/YSZ interface had no extensive contact points with visible neck formations (see Fig. 20). The Pd grains seem to make only a mechanical contact with the electrolyte. The high open porosity makes it reasonable to assume that the gas has access everywhere except in the region between the Pd and the YSZ. Compared to the Pt electrodes, since the Pd grains did not wet the electrolyte surface, the non-wetting grain could lead to a slight increase in the gas-phase mass

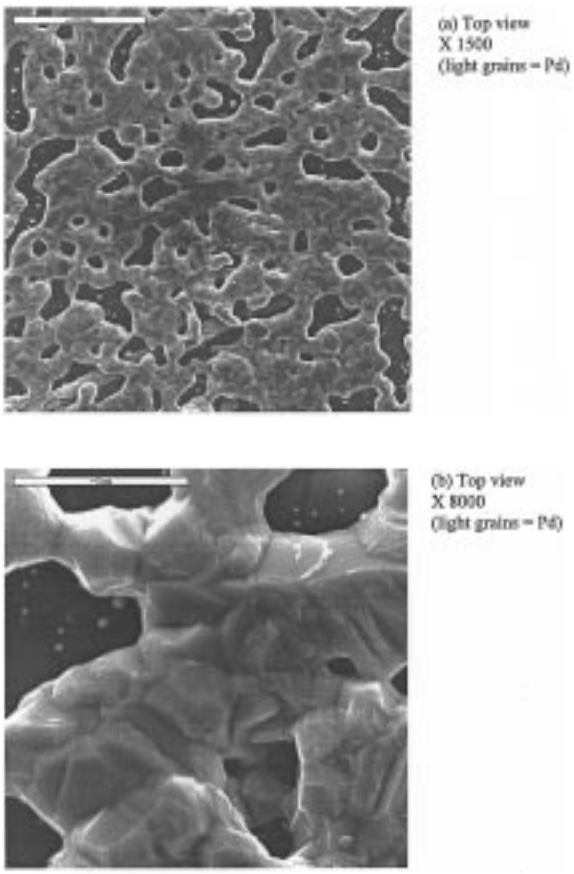

Fig. 19. Top view of the open porosity.

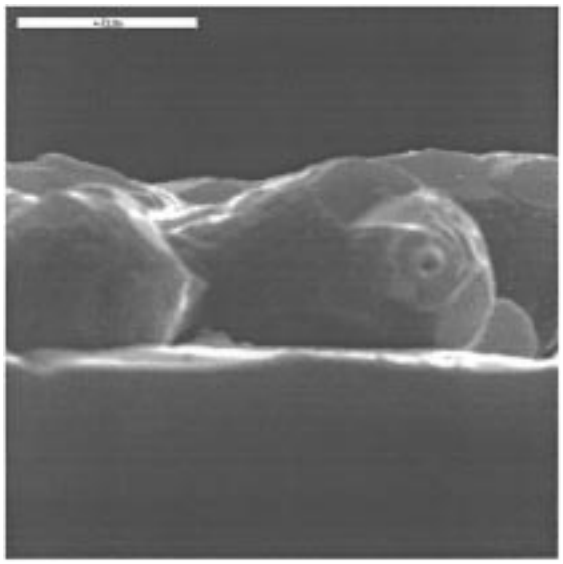

Fig. 20. Cross section of the Pd/YSZ interface at magnification × 15000.

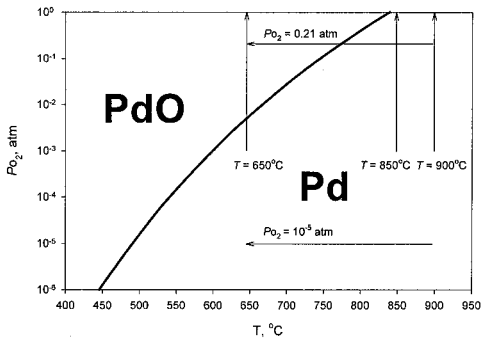

Fig. 21. The Pd/PdO phase diagram and the 5 sets of steady-state measurements (each set represents discrete measurements in a range indicated by the lines and the general order in which the measurements were made is indicated by the arrows).

transfer resistance by decreasing the effective oxygen-gas diffusivity in the electrode.

Effect of P_{O_2} and temperature. Figure 21 shows the Pd/PdO phase diagram at 1 atm total pressure. Three sets of isothermal-interfacial-impedance measurements (900, 850, and 650°C) were made at discrete values of P_{O_2} ranging from 0.02 to 1 atm. As seen in Fig. 21 at 900°C and 850°C Pd is stable in the entire range, whereas at 650°C PdO is stable only at high P_{O_2}. Two sets of isobaric measurements were made ($P_{O_2} = 10^{-5}$ and 0.21 atm) at discrete values of T, ranging from 900 to 650°C.

Apart from a resistive element at high frequencies, the impedance spectra consist of two separated arcs (I and II in Fig. 22). The high frequency intercept is attributed to the ohmic drops. At higher temperatures and low P_{O_2}, in the absence of PdO, the two arcs are clearly visible, although there is a slight overlap and the intersection is at 62 Hz. The arcs can be interpreted with the circuit shown in Fig. 22. The extrapolated real-axis intercept of the first arc is $R_p^{(1)}$, and that of the second arc is $R_p^{(2)}$. The origin of the first arc, as in the case of Pt, is due to the charge-transfer step, and the second arc which is not visible for Pt, is due to a mass-transfer step as discussed in the ''Theory'' section.

A typical temperature dependence of the impedance of the Pd/YSZ interface is shown in Figs. 23 and 24. Both arcs increase with decrease in temperature, but arc I is more strongly dependent on

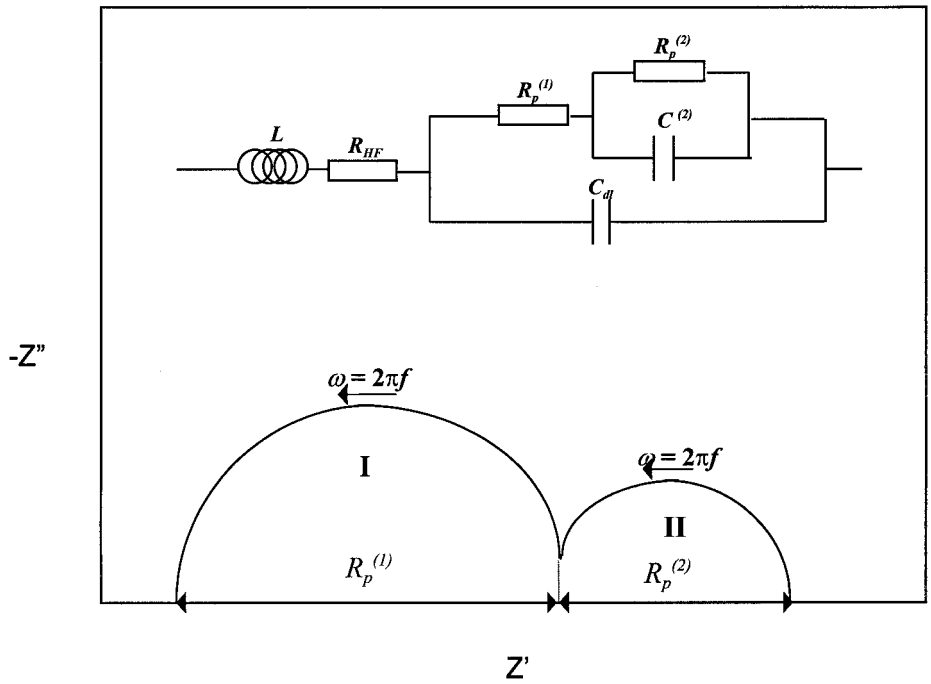

Fig. 22. Representative impedance spectra of the Pd/YSZ interface.

the temperature than arc II. Also, both $R_p^{(1)}$ and $R_p^{(2)}$ decrease as P_{O_2} increases; $R_p^{(2)}$ decreases at a faster rate than $R_p^{(1)}$.

Tables 2 and 3 summarize the kinetic data in the region where PdO is thermodynamically unstable. C_{dl} is identified as the double layer capacitance due to its invariance with respect to P_{O_2}. Its magnitude is comparable to the double layer values reported for Pt/YSZ interfaces. The basis for analytical fitting was the circuit shown in Fig. 22. The impedance spectra of the Pd/YSZ interface were compared with the reaction models presented before. The faradaic portion can be

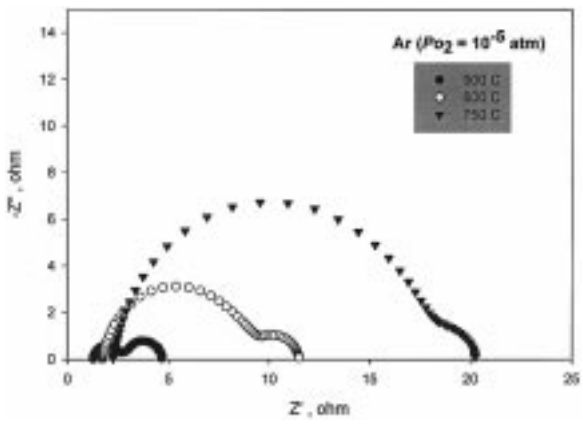

Fig. 23. Spectra for the Pd/YSZ interface at different temperatures in argon.

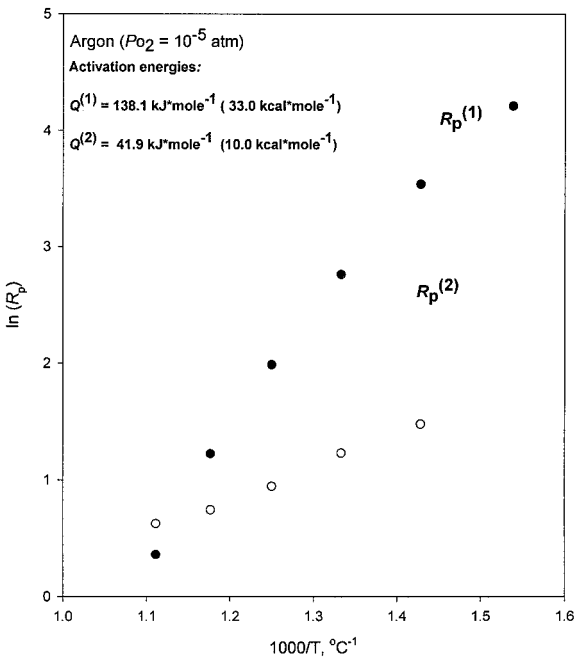

Fig. 24. Temperature dependence of $\ln(R_p)$ under argon.

Table 2. Summary of the resistive elements in the impedance data where PdO is thermodynamically unstable

Element	Q (kJ/mole)	m, $[R_p = (P_{O_2})^m]$
$R_p^{(1)}$	144 ± 6	-0.37 ± 0.05
$R_p^{(2)}$	$42 \pm (5)$	-0.93 ± 0.02

Table 3. Summary of the capacitive elements in the impedance data where PdO is thermodynamically unstable

Element	P_{O_2} dependence	T dependence	Range
C_{dl}	no dependence	no dependence	$100\,\mu$F
$C^{(2)}$	increase with increasing P_{O_2}	increase with decreasing T	0.04–0.7 F

decomposed into a purely ohmic part, R_{ct}, and a pseudocapacitive/resistance combination, Z_{mt}. All circuits indicated that the diameter of the high frequency arc equaled R_{ct}. The low frequency capacitive element (related to $C^{(2)}$) was much bigger (3–4 orders of magnitude) and thus, all faradaic components, except R_{ct}, were shorted at high frequencies. $R_p^{(1)}$ was therefore taken as R_{ct} and could be expressed as $(P_{O_2})^m$ where m was -0.37 ± 0.05. This agrees with Langmuir dissociative adsorption model for low surface coverage (Eq. (10)). The activation energy of the charge transfer process, E_r, can be calculated from the apparent activation energy Q using Eq. (11). For the dissociative adsorption of oxygen on palladium, ΔH_{ads} has been reported to be 294 kJ/mole [24]. E_r is then 253 kJ/mole. The resistive element in the low-frequency impedance arc, $R_p^{(2)}$, has a P_{O_2} dependency close to -1 and a smaller thermal activation compared to $R_p^{(1)}$ (Table 2). These trends are consistent with gas-phase-diffusion impedance [37–39]. Also, the estimated values of $R_p^{(2)}$ considering gas-phase diffusion

$$\left(R_p^{(2)} \approx \left(\frac{RT}{4F}\right)^2 \frac{h}{P_{O_2} D_{O_2}}\right)$$

through an electrode having a thickness (h) similar to that employed in the present study (1–15 microns), agree with the small values of $R_p^{(2)}$ obtained from the measurements; for the estimation of $R_p^{(2)}$ an oxygen diffusivity value of $0.5\,cm^2/s$ [37] was used. These observations lend credence to the fact that the lower-frequency-impedance response may be due to a gas-phase diffusion limitation in the electrode.

It may be noted that the other three models described earlier for mass transport were also fitted to the measured spectra. All the circuit models simulated the two separated arcs I and II well. As an example, the simulation with lateral diffusion is shown in Fig. 25. However, the simulations do not entirely agree with the primary criterion that the P_{O_2} and temperature dependencies should be consistent with the physical process.

The effect of P_{O_2} on R_p $(R_p = R_p^{(1)} + R_p^{(2)})$ at 650°C is shown in Fig. 26. At 650°C, when Pd is not significantly oxidized, $R_p^{(2)}$ is insignificant in comparison to $R_p^{(1)}$ (thus, $R_p \approx R_p^{(1)}$). From Fig. 21, it can be seen that PdO is thermodynamically stable at P_{O_2} greater than 7.10^{-3} atm. At about $P_{O_2} = 0.04$ atm $(\log P_{O_2} = 1.4)$, there is an abrupt increase of R_p with P_{O_2} (see Fig. 26). This increase is most probably due

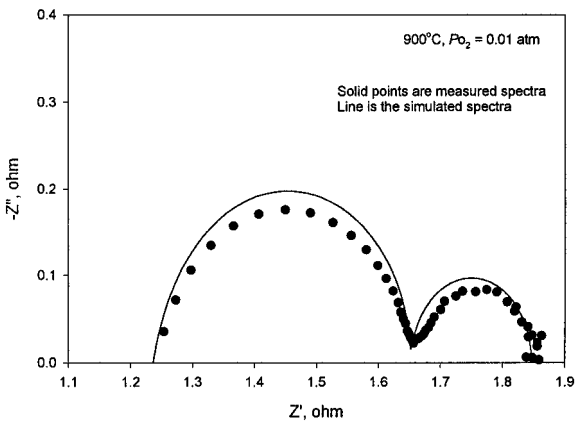

Fig. 25. Simulated spectrum using Eq. (15) vs. real spectrum.

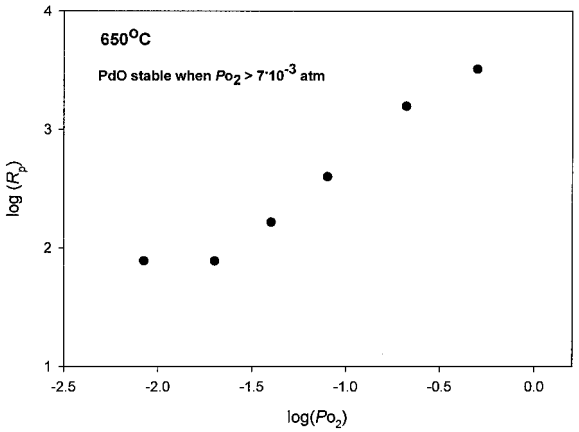

Fig. 26. The dependence of the polarization of log (P_{O_2}) at 650°C.

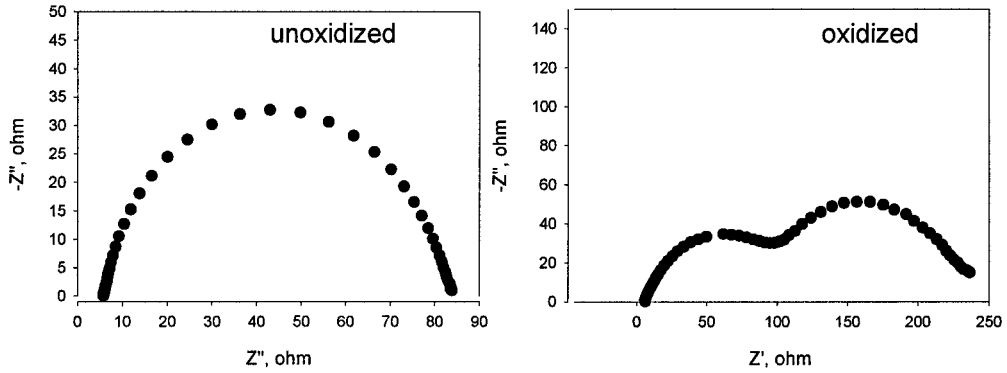

Fig. 27. Impedance spectra of Pd/YSZ at $P_{O_2} = 0.02$ atm and 650°C

to the onset of oxidation. The delay in the onset is likely to be due to kinetic reasons.

In order to study the effect of electrode oxidation on the impedance response, two spectra are needed under identical conditions of P_{O_2} and temperature: one taken prior to any oxidation, and the other recorded after the oxidation processes are either completed or have practically halted due to kinetic reasons. In order to create these two situations, the following experiments were carried out. The cell was exposed to pure O_2 at 650°C until the spectra were stable with time. The system was then brought back to $P_{O_2} = 0.02$ atm $(\log P_{O_2} = -1.7; T = 650°C)$. PdO is stable under these conditions and hence did not decompose. The impedance of the oxidized electrode was then compared to the state of the interface at $P_{O_2} = 0.02$ atm while raising the P_{O_2} from a value where no oxidation was observed. In this case, although the oxide was stable at $P_{O_2} = 0.02$ atm, no oxidation was observed due to kinetic reasons. Figure 27 shows the remarkable difference in shape of the spectra between the two states. The two states must be represented with different electrical models. Before oxidation, the arc is simply modeled as a Randles circuit. This is possible since $R_p^{(2)}$ is negligible, as described above. After significant oxidation, the impedance must be deconvoluted to include the mass transport component associated with the change induced by oxidation. It is possible that with the oxidized Pd, the oxygen-gas diffusivity in the electrode decreases and causes the lower-frequency response to become prominent.

Effect of oxidation in air at 650°C. In order to study the influence of PdO on the exchange reaction, an experiment was done where an unoxidized sample was oxidized in air at 650°C. The evolution of the total overall polarization R_p $(R_p = R_p^{(1)} + R_p^{(2)})$ is shown in Fig. 28 as a function of time in a logarithmic scale. Figure 29 shows a thermogravimetric measurement of the oxidation of Pd under the same conditions. As seen from Fig. 29, after about 1% weight increase, the oxidation becomes very slow. The decay in the diffusion rate could be due to the fact that a diffusion-limited process becomes rate-limiting after the surface has been covered with an oxide layer.

The increase in R_p shown in Fig. 28 is primarily due to $R_p^{(1)}$. This can be rationalized considering the fact that the oxygen partial pressure is high (air) and appreciable oxidation has not taken place. Furthermore, since PdO is a good semi-conductor above 227°C [40], no increase in the ohmic resistance was observed; the high-frequency real axis intercept of the impedance spectra did not increase during oxidation.

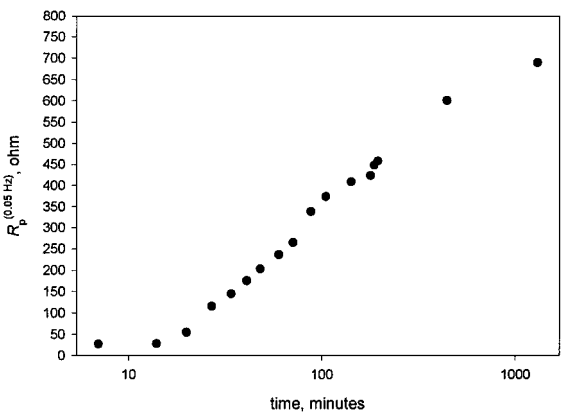

Fig. 28. Polarization change with time after exposing the electrode to air at 650°C.

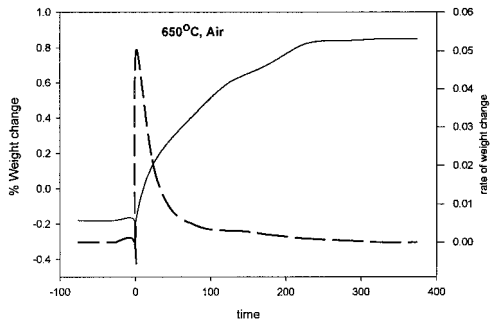

Fig. 29. Thermogravimetric data of Pd in air at 650°C. The solid line shows weight change with time and the dashed line shows the rate of weight change with time.

The most plausible cause for the increase in R_p during oxidation is a drastic change in the electrocatalytic properties of the electrode, caused by the surface layer of PdO that forms.

Figure 29 shows, however, that the oxidation stops (or becomes very slow) after about 400 min. This means that R_p vs. time should also stop increasing after 400 min. However, Fig. 28 shows that R_p continues to rise even after 400 min (although at a decreasing rate). The difference could be due to the fact that the electrode provides a gas-phase-diffusion resistance as it oxidizes. This is consistent with our earlier observations on the lower-frequency-impedance response. Also as the PdO is less electrocatalytic than Pd, the impedance continues to increase as the interface is being covered with PdO.

Effect of direct current. The influence of direct current on the interfacial impedance spectrum was investigated in two ways: under isobaric and isothermal conditions. The rationale for varying the temperature and P_{O_2} is the following: if the current-induced effect is related to the formation/decomposition of Pd-O compounds, then the stability of PdO should influence the magnitude of this effect. According to Fig. 21, an anodic current should have a larger effect at higher P_{O_2} and/or lower temperature since the Pd-O compounds are more stable under these conditions. Anodic currents of 10 mA were passed for 5 min to study the possible effects on the interfacial impedance after current interruption. At 900°C (in air) there was no effect on the impedance since the formation of Pd-O compounds is not favored. At 700°C the current-induced change was clearly observable as shown in Fig. 30. After current interruption, there was a recovery period in which the impedance shrank. The final steady-state spectrum was larger than the original spectrum. From Fig. 21 it can be seen that PdO is thermodynamically stable in air at 700°C. It is therefore conceivable that the anodic-current-induced effect at this temperature is associated with the formation of PdO since the formation of PdO increases the electrode impedance by affecting the electrocatalytic properties of the Pd/YSZ interface. The current-induced change in the interfacial impedance is shown at different P_{O_2} values in Fig. 30. At $P_{O_2} = 0.21$ and 0.12, the magnitude of the increase and the remanent hysteresis of the interfacial impedances were comparable. At lower P_{O_2}, however, the current-induced effect decreased. This is reasonable since the OCS formation is expected to be favored under more oxidizing conditions.

Comparison between Pd-YSZ and Pt-YSZ

When PdO is thermodynamically unstable, the oxygen exchange at the Pd/YSZ interface proceeds according to a mixed mechanism of charge transfer (high-frequency-impedance response) and gas-phase mass transfer in the electrode (low-frequency-impedance response). When PdO is thermodynamically stable and the electrode surface oxidized, the oxygen exchange across Pd/YSZ is partially blocked due to poor catalytic properties of PdO and the gas-phase diffusion resistance increases. The current-induced effect on the oxygen-exchange reaction is observable under the conditions when PdO is thermodynamically stable. The polarization shift due to anodic currents increases with decrease in temperature and increase in P_{O_2} due to OCS formation at the charge-transfer sites.

The model presented for the Pt-YSZ interface stated that the current induced impedance change is due to the formation/depletion of OCS at the charge transfer sites. The presence of OCS lowers the rate of the oxygen-exchange reaction. If PdO is part of the OCS that influences the reaction sites, then the model predicts that the current-induced modification of the interfacial impedance should be more prevalent when PdO is thermodynamically stable. The results on Pd/YSZ system show that the impedance increase due to OCS formation is mainly present in the T and P_{O_2} regimes where PdO is stable. The experiments thus confirm the model or the hypothesis.

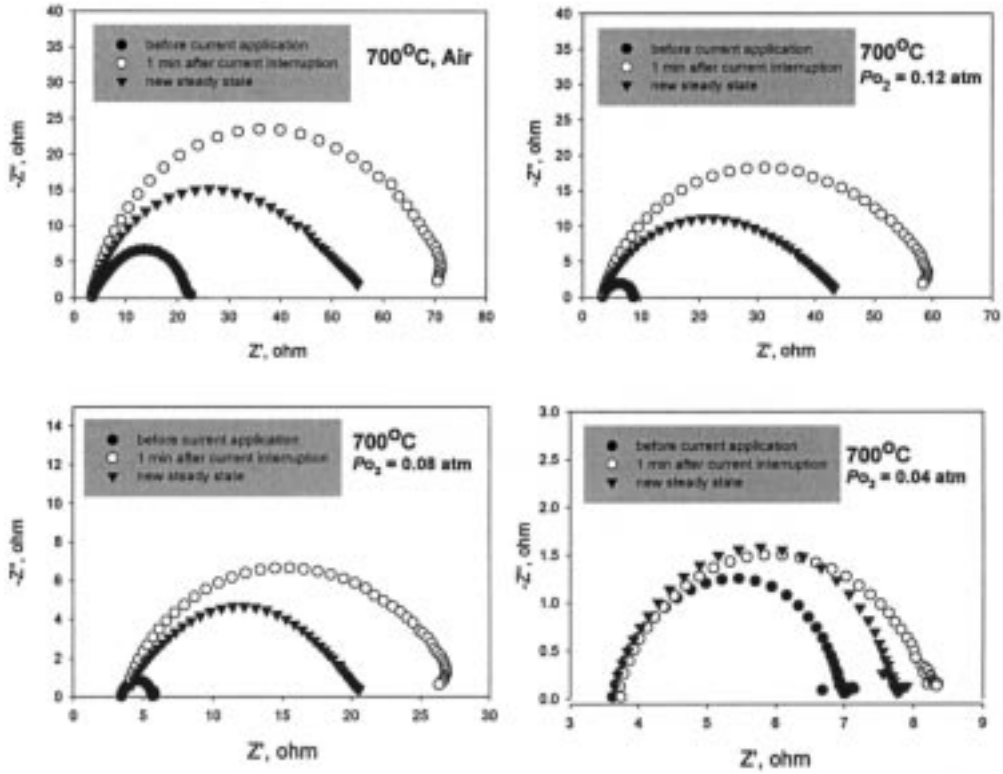

Fig. 30. Effect of an anodic current of 10 mA passed for 5 min on the impedance spectra of the Pd/YSZ interface.

At low P_{O_2}, the impedance response of the Pd/YSZ interface consists of two semi-circles. The first (high-frequency response) is related to charge transfer and the second (lower-frequency response) is related to gas-phase diffusion. In the case of Pt/YSZ interface, only the response related to the charge transfer step is clearly observed. This may be due to the fact that the Pt wets the YSZ substrate and the Pd does not. The non-wetting nature of Pd may result in increasing the gas-phase-diffusion impedance and hence explain the low-frequency response. It is also possible that the low-frequency response is not observed for the Pt/YSZ interface because the timescales are less resolved. The pseudocapacitance of Pt/YSZ interface is much lower than the Pd/YSZ interface due to differences in OCS.

Conclusions

The effect of temperature, oxygen partial pressure, current and electrode microstructure on the interfacial impedance of Pt/$(Y_2O_3)_{0.08}(ZrO_2)_{0.92}$ and Pd/$(Y_2O_3)_{0.08}(ZrO_2)_{0.92}$ has been studied. The change in oxygen concentration due to oxygen supply/depletion induced by direct current was studied by monitoring the impedance in the time domain after current interruption. It is shown that the kinetics of the charge-transfer reaction is influenced by variations in the oxygen-chemical potential at the charge-transfer sites. The reason for this is that the metal (Pt or Pd) at the charge-transfer sites (triple-phase boundaries between gas/YSZ/metal) react with oxygen to form oxygen-containing species (OCS). As a result of this reaction, the electrocatalytic properties that govern the kinetics of the exchange reaction are altered.

Near-equilibrium experiments show that at the Pt/$(Y_2O_3)_{0.08}(ZrO_2)_{0.92}$ interface the charge-transfer reaction obeys a P_{O_2} dependence in agreement with a Langmuir adsorption isotherm. When heating from room temperature, the impedance spectra are modified after passing direct currents. Anodic currents increase the interfacial impedance and cathodic

currents decrease it. Anodic currents increase the OCS concentration by supplying oxygen to the TPB. Therefore, the interfacial impedance increases after anodic currents. Cathodic currents deplete oxygen from the TPB and thereby lower the OCS concentration. This results in a decrease in the interfacial impedance. The observed decrease in impedance with time at 1050°C is linked to the decomposition and stripping of the OCS. Due to the OCS-stripped state of the Pt/YSZ interface, the interfacial impedance is smaller when the cell is cooled from 1050°C compared to when it is heated from room temperature. Upon cooling the current-induced modification of the impedance for the OCS-stripped interface is absent until the system is cooled below 850°C and the OCS reappears.

The impedance for the $Pd/(Y_2O_3)_{0.08}(ZrO_2)_{0.92}$ interface near equilibrium conditions, consists of two semi-circles. An analysis of the P_{O_2} and temperature dependencies show that the first one is related to the charge-transfer at the TPB and the second arc to the gas-phase diffusion in the electrode. The P_{O_2} dependency of the charge-transfer resistance show that dissociative Langmuir adsorption is obeyed. When PdO is thermodynamically stable, the charge-transfer impedance increases with time due to PdO formation leading to a lowering of the electrocatalytic properties of the electrode. When the Pd electrode is significantly oxidized, the mass-transfer impedance also increases. The current-induced impedance change is observable within the stability region of PdO. This suggests that PdO is the OCS at the $Pd/(Y_2O_3)_{0.08}(ZrO_2)_{0.92}$ interface.

Acknowledgments

The Exploratory Program of the Electric Power Research Institute supported this work. The authors thank Prof. Harry L. Tuller for his helpful suggestions and input during the course of this work at MIT.

References

1. H.-D. Wiemhofer, *Ber. Bunsenges. Phys. Chem.*, **97**, 461 (1993).
2. H.-D. Wiemhofer, *Solid State Ionics*, **75**, 167 (1995).
3. G.B. Barbi, *Ber. Bunsenges. Phys. Chem.*, **99**, 741 (1995).
4. E. Siebert, *Electrochimica Acta.*, **39**, 1621 (1994).
5. B.C.H. Steele, *Solid State Ionics*, **75**, 157 (1995).
6. C. Schwandt and W. Weppner, *J. Electrochem. Soc.*, **144**, 3728–3738 (1997).
7. S. Sridhar, V. Stancovski, and U. Pal, *J. Electrochem. Soc.*, **144**, 2479–2485 (1997).
8. I. Samsonov and G. Valentinovich, *The Oxide Handbook* (Plenum Press, NY, 1982).
9. J.L. Gland, *Surface Science*, **93**, 487 (1980).
10. J.L Gland, B.A. Sexton, and G.B. Fisher, *Surface Science*, **95**, 587 (1980).
11. G.A. Somorjai, *Chemistry in Two Dimensions—Surfaces*, (Cornell University Press, Ithaca and London, 1981), p. 500.
12. B.L. Kuzin and M.A. Komarov, *Solid State Ionics*, **39**, 163 (1990).
13. B.J. Berry, *Surface Science*, **120**, 409 (1982).
14. C.G. Vayenas and N. Michaels, *Surface Science*, **120**, 405 (1982).
15. O.J. Velle, T. Norby, and P. Kofstad, *Solid State Ionics*, **47**, 161 (1991).
16. Ihsan Barin, *Thermodynamic Data of Pure Substances*, VCH, 1168 (1993).
17. Cl. Duval, *Inorganic Thermogravimetric Analysis* 2nd edition (Elsevier, Amsterdam, 1963), p. 586.
18. S.P.S. Badwal and H.J. de Bruin, *J. Electrochem. Soc.*, **129**, 1921 (1982).
19. J. Van Herle and A.J. McEvoy, *Ber. Bunsenges. Phys. Chem.*, **97**, 470 (1993).
20. S. Sridhar, Ph. D. Thesis (MIT Cambridge, MA, 1997).
21. T.H. Etsell and S.N. Flengas, *J. Electrochem. Soc.*, **118**, 1890 (1971).
22. T.M. Gür, I.D. Raistrick, and D.A. Huggins, *J. Electrochem. Soc.*, **127**, 2620 (1980).
23. D. Braunshtein, D.S. Tannhauser, and I. Riess, *J. Electrochem. Soc.*, **128**, 82 (1981).
24. J.R. Anderson, *Structure of Metallic Catalysts* (AP Press, NY, 1975), p. 13.
25. J.E. Bauerle, *J. Phys. Chem. Solids*, **30**, 2657 (1969).
26. F.K. Moghadam and D.A. Stevenson, *J. Electrochem. Soc.*, **133**, 1329 (1986).
27. S. Pizzini, *Fast Ionic Transport in Solids*, ed. by W. van Gool, (North Holland Press, Amsterdam, 1973), p. 461.
28. J. Mizusaki, K. Amano, S. Yamauchi, and K. Fueki, *Solid State Ionics*, **22**, 323 (1987).
29. D.Y. Wang and A.S. Nowick, *J. Electrochem. Soc.*, **128**, 55 (1981).
30. J.R. Macdonald, *Impedance Spectroscopy—Emphasizing Solid Materials and Systems* (John Wiley, 1987), p. 71.
31. P.G. Bruce, *Solid State Electrochemistry* (Cambridge University Press, 1995).
32. A.J. Winnubst, A.H.A. Scharenborg, and A.J. Burggraaf, *Solid State Ionics.*, **14**, 319 (1984).
33. M.J. Ververk and A.J. Burggraaf, *J. Electrochem. Soc.*, **130**, 76 (1983).
34. J. Bockris and A.K.N. Reddy, *Modern Electrochemistry* Vol. 2, Chapter 9 (1977).
35. D.R. Franceschetti and A.P. Ross, *Appl. Phys. A.*, 49, 111 (1989).

36. D.Y Wang and A.S. Nowick, *J. Electrochem. Soc*., **126**, 1166 (1979).
37. J.A. Lane, S. Adler, P.H. Middleton, and B.C.H. Steele, *Solid Oxide Fuel Cells IV*, ed. by M. Dokiya, O. Yamamoto, H. Tagawa, and S.C. Singhal, ECS (Pennington, New Jersey, 1995), p. 584.
38. S.B. Adler, J.A. Lane, and B.C.H. Steele, *J. Electrochem. Soc*., **143**, 3554 (1996).
39. A.M. Svensson, S. Sunde, and K. Niscancioglu, *J. Electrochem. Soc*., **144**, 2719 (1997).
40. H. Okamoto and T. Aso, *Japanese J. Appl. Phys*., **6**, 779 (1967).